Two-loop calculations with vertex corrections in the Walecka model

Brian D. Serot
Physics Department and Nuclear Theory Center, Indiana University, Bloomington, Indiana 47405

Hua-Bin Tang
Department of Physics, The Ohio State University, Columbus, Ohio 43210
(Received 18 April 1994)

Two-loop corrections with scalar and vector form factors are calculated for nuclear matter in the Walecka model. The on-shell form factors are derived from vertex corrections within the framework of the model and are highly damped at large spacelike momenta. The two-loop corrections are evaluated first by using the one-loop parameters and mean fields and then by refitting the total energy/baryon to empirical nuclear matter saturation properties. The modified two-loop corrections are significantly smaller than those computed with bare vertices. Contributions from the anomalous isoscalar form factor of the nucleon are included for the first time. The effects of the implicit density dependence of the form factors, which arise from the shift in the baryon mass, are also considered. Finally, necessary extensions of these calculations are discussed.

PACS number(s): 21.30.+y, 21.60.Jz, 21.65.+f

I. INTRODUCTION

The traditional theory of nuclear structure is based on the Schrödinger equation with a nucleon-nucleon (NN) potential that has its origin in meson exchange. In this nonrelativistic approach, one fits the NN potential to the empirical properties of the deuteron and to low-energy NN scattering data, and one then attempts to predict the behavior of many-nucleon systems. A natural and appealing generalization of this approach is to incorporate special relativity by using a relativistic quantum field theory with explicit meson and baryon degrees of freedom. These degrees of freedom are chosen because they are the most efficient for describing low- and medium-energy nuclear experiments. This generalization allows us to study interacting, relativistic, nuclear many-body systems, which future experiments will examine. The two basic questions are: what kind of field theories should we use, and how well can we describe nuclear systems using field theoretical models with hadrons, which are actually particles with internal structure? These are broad and hard questions that can be answered only after intensive and systematic investigation.

Renormalizable relativistic quantum field theories with hadronic degrees of freedom, often called *quantum hadrodynamics* or QHD, have been studied for some time [1–3]. At the level of the mean-field theory (MFT) and one-loop approximation ("relativistic Hartree approximation" or RHA), these models can reproduce nuclear matter saturation and can realistically describe many bulk and single-particle properties of finite nuclei [2–4]. The dynamical assumption behind renormalizability in QHD is that the quantum vacuum and the internal structure of the hadrons can be described in terms of hadronic degrees of freedom alone. This assumption must ultimately break down at very short distances, and its limitations can be tested by explicit calculations.

Some approximate QHD calculations beyond the one-loop level [5–8] indicate large vacuum corrections, and even the validity of the one-loop vacuum contribution has been questioned [9]. However, it is unlikely that we can calculate consistently beyond the mean-field level by introducing *ad hoc* procedures, such as including only the nucleons in the Fermi sea and simply throwing away Dirac-sea contributions. Indeed, it is already known that vacuum contributions are indispensable for maintaining the conservation of momentum and the electromagnetic current at the level of the random-phase approximation (RPA) [10,11]. These results imply that we must develop practical and reliable techniques that go beyond the MFT and that include vacuum dynamics.

A straightforward two-loop approximation for nuclear matter in the Walecka model was examined in Ref. [5], where large vacuum corrections were found. The loop expansion does not appear to be convergent or asymptotic in any sense. This is not a surprise if we notice that the two-loop corrections are essentially perturbative in the large couplings. An alternative expansion in terms of meson loops (after integrating out the baryon fields) encounters the well-known ghost problems [6–8]. The ghost poles can be removed by using Redmond's procedure [12], but the vacuum contributions are still too large [8,13]. These calculations suggest that vertex corrections (and short-range correlations) should be included to compute vacuum loops reliably in QHD theories [14].

Since hadrons have internal substructure, one could argue for the use of nonlocal couplings and the introduction of *ad hoc* vertex form factors. This procedure was adopted in Refs. [15–17]. We remark that the introduction of form factors implies nonrenormalizability of the theory from the outset, and thus the renormalization procedure in Refs. [15] and [16] needs justification. (In other words, various subtractions were made in the computation of the energy that arise naturally only in a renormal-

izable theory.) This *ad hoc* procedure also says nothing about off-shell or density-dependent effects. Moreover, although QCD in principle gives a complete description of nucleon structure, some part of the internal properties of the nucleon, particularly at large distances, must be equivalent to that provided by virtual hadron loops. These are the physical effects we intend to study in this paper.

As pointed out recently by Milana [14], a theory with baryons and vector mesons contains proper vertex functions that are highly damped at large spacelike momentum transfers, due to the contributions from virtual bremsstrahlung summed to all orders. This damping arises from the long-range (infrared) structure of the vertex and so should be calculable within the QHD framework. Since the QHD theory is renormalizable, the vertex function can be expressed in terms of the couplings and masses of the theory, with no *ad hoc* parameters. Although it may be impossible to achieve a truly quantitative description of the hadron structure within a QHD model, due to the complicated nature of the vertex functions, our goal is to understand at least the qualitative features of the vertex functions implied in a hadronic theory and to see how these features affect calculations with vacuum loops.

In a recent calculation [18], the on-shell vector form factor was studied in a model with baryons and vector mesons. The behavior at large spacelike momentum transfer Q was determined by the leading logarithmic infrared behavior, which arises from the sum of all diagrams with vector ladders and crossed ladders across the hard vertex. At small Q, the lowest-order vertex correction was used, and the complete vertex function was constructed by interpolating smoothly between the low- and high-momentum-transfer regimes. (See Ref. [19] for a similar analysis with a somewhat different strategy.)

In this paper we extend the method of Ref. [18] to the scalar-baryon vertex and apply the form factors so obtained to two-loop calculations in the Walecka model, with the Lagrangian density

$$\begin{aligned}\mathcal{L} = {} & \bar{\psi}(i\partial\!\!\!/ - g_v V\!\!\!/ - M + g_s\phi)\psi \\ & + \tfrac{1}{2}(\partial_\mu\phi\partial^\mu\phi - m_s^2\phi^2) \\ & - \tfrac{1}{4}F_{\mu\nu}F^{\mu\nu} + \tfrac{1}{2}m_v^2 V_\mu V^\mu + \delta\mathcal{L} \ , \end{aligned} \tag{1.1}$$

where $F^{\mu\nu} = \partial^\mu V^\nu - \partial^\nu V^\mu$ and $\delta\mathcal{L}$ contains the counterterms. We observe that the *off-shell* vertex functions should be used in a fully satisfactory calculation with loops. A full off-shell calculation is quite complicated, however, as one needs to know the off-shell behavior of the vertices at all spacelike momenta, as well as the modification of the vertices in the presence of valence nucleons at finite density. Calculations exploring these off-shell vertex functions are in progress [20]. Here, as a first step, we use an on-shell approximation, in which the off-shell vertex functions are replaced by their on-shell forms at zero density. This procedure is analogous to that used in Refs. [15] and [16], where parametrized, on-shell form factors were used at the vertices, except that we use form factors obtained from within our model. Note also that the form factors used in Refs. [15] and [16] were chosen to have simple momentum dependence, which allowed the two-loop energy to be calculated directly from the results of Ref. [5]; in contrast, we allow for an *arbitrary* momentum dependence in the form factors, which requires us to implement a different renormalization procedure for the two-loop contributions. Moreover, the anomalous vector form factor is included here in the two-loop results for the first time. Finally, we also estimate the effects of the implicit density dependence due to the effective nucleon mass M^* that appears in the integrals that define the form factors.

To include the form factors systematically, we apply the method of Freedman and McLerran [21] to nuclear matter in the Walecka model. One of the approximations that can be developed from this formalism is a two-loop approximation with one dressed vertex [13]. Using this approximation, we calculate the corrections to the one-loop energy: first by using the coupling parameters and mean fields determined at the one-loop level and then by refitting the total energy to the empirical nuclear matter saturation properties. We find that the behavior of the two-loop corrections is significantly improved compared to that obtained with bare vertices [5]. (This agrees with results obtained in calculations with *ad hoc* vertex functions [15,16].) The contribution from the vector anomalous vertex is small compared to those from the vector charge and scalar vertices, but not negligible. The effects of the M^* dependence and of the uncertainty in our interpolations for the form factors are modest compared to the overall size of the two-loop corrections, but are nevertheless significant on the scale of the nuclear matter binding energy. These new effects, which are usually neglected in studies using *ad hoc* form factors, are therefore important for a detailed description of the saturation properties of nuclear matter, because of the sensitive cancellations in the energy that occur near equilibrium density. It will certainly be necessary to extend our calculations to include the integrations over the off-shell vertex functions before any definitive statements can be made about nuclear matter saturation in this model.

We emphasize that the basic motivation for the present work is to make some qualitative statements about the role of vertex modifications that arise within the framework of the Walecka model. The meson-baryon vertex functions are highly damped at large spacelike momenta [14,18], so it is necessary to include them in loop integrals for the energy density. The inclusion of dynamical vertex functions leads to significant new complications in the evaluation of the energy of nuclear matter; similar complications would arise regardless of the degrees of freedom used. These new problems are usually not discussed in calculations using *ad hoc* vertex functions, and many of them are not resolved here; we make several important approximations whose validity can be tested only by extending our calculations, as discussed in the Summary. Nevertheless, we arrive at finite expressions for the nuclear matter energy density that contain vertex form factors calculated within the model, and we expect that these results are adequate for a qualitative discussion of the impact of these vertex functions on the size of the two-loop corrections.

Some remarks are also in order about our calculation of vacuum fluctuations involving the scalar field. Here we treat the scalar field that represents the σ meson as "elementary," although it should, as generally believed, be considered as simulating the exchange of two correlated s-wave pions [22–25]. Our goal in this work is to develop tools for calculating vacuum corrections in a model with an NN interaction that has short-range repulsion and midrange attraction, as is empirically observed. The Walecka model is a simple one that satisfies this constraint. A more complete discussion of the role of chiral symmetry and of the dynamical generation of the midrange NN attraction, together with the implications for vacuum loops, should be considered as a necessary refinement of the work presented here [3,25]. It is possible that a more detailed treatment could modify our results significantly, but it is also possible that a simple scalar field could remain an adequate approximation to correlated two-pion exchange even for the calculation of vacuum loops. We leave these extensions as topics for future study.

The rest of this paper is organized as follows. In Sec. II we discuss the renormalization of the energy corrections in the two-loop approximation with one dressed vertex. The finite expressions that are used in our numerical calculations are generated. In Sec. III we present our approximations for the vertex functions and the method for determining the on-shell form factors. The results for the energy of nuclear matter with the vertex functions fixed at their free-space forms are given in Sec. IV, and we study the effects of medium-modified vertices in Sec. V. Section VI is a summary, and some technical details are included in an Appendix.

II. TWO-LOOP APPROXIMATION WITH VERTEX CORRECTIONS

To include vertex functions in loop calculations of the nuclear matter energy density, it is convenient to apply the method of Freedman and McLerran [21], in which the thermodynamic potential is constructed as a function of the full, connected propagators and proper vertices that satisfy the Schwinger-Dyson equations. By truncating the expansion of the thermodynamic potential and the Schwinger-Dyson equations appropriately, we can obtain various well-known approximations, such as the MFT, the RHA, the straightforward two-loop approximation [5], the relativistic RPA, etc. Details of these formal procedures are reported elsewhere [13,26]. Here we merely quote the results for the two-loop approximation with one dressed vertex.

Although the method of Freedman and McLerran provides for systematic truncation, it says nothing about the best way to approximate the exact thermodynamic potential in the case of strong couplings. It is also possible to truncate the expansion to include dressed vertices at *both* ends of the two-loop diagram. Here we shall take a conservative approach and include only one dressed vertex; if this gives adequate suppression of the vacuum loops, two dressed vertices will give even more. The question of which of these truncations is a better starting point can be answered only by including the next term in the expansion, and we leave this as a topic for future study.

At the one-loop level (or RHA), the nuclear matter energy density can be written as [2]

$$\mathcal{E}^{(1)} = \frac{g_v^2}{2m_v^2}\rho_B^2 + \frac{m_s^2}{2g_s^2}(M-M^*)^2 + \frac{\gamma}{(2\pi)^3}\int^{k_F} d^3k\, E_k^* + \Delta\mathcal{E}(M^*)\,, \tag{2.1}$$

where $E_k^* \equiv (\mathbf{k}^2 + M^{*2})^{1/2}$ and $M^* = M - g_s\phi_0$, with ϕ_0 the average scalar field. The spin-isospin degeneracy $\gamma = 4$ for nuclear matter and $\gamma = 2$ for neutron matter, and the mean vector field has been eliminated using

$$V_0 = \frac{g_v}{m_v^2}\rho_B \equiv \frac{g_v}{m_v^2}\frac{\gamma k_F^3}{6\pi^2}\,, \tag{2.2}$$

since it is a constant of the motion. The one-loop vacuum correction ("zero-point energy") is

$$\Delta\mathcal{E}(M^*) = -\frac{1}{4\pi^2}\Big\{M^{*4}\ln(M^*/M) + M^3(M-M^*) - \tfrac{7}{2}M^2(M-M^*)^2 + \tfrac{13}{3}M(M-M^*)^3 - \tfrac{25}{12}(M-M^*)^4\Big\}, \tag{2.3}$$

where the renormalization conditions of Chin [27] have been used, and we have assumed that $\gamma = 4$ for the Dirac sea.

The two-loop approximation with one dressed vertex obtained using the method of Freedman and McLerran is most transparently described by Feynman diagrams. The two-loop corrections to the RHA energy density can be drawn as in Fig. 1, where Σ denotes the renormalized proper baryon self-energy shown in Fig. 2, and Λ_s (Λ_v) stands for the dressed scalar (vector) vertex. The square brackets indicate that the enclosed subdiagrams are renormalized by the inclusion of the appropriate subtractions. (We follow the diagrammatic conventions of Ref. [21].)

The propagators in Fig. 1 are as follows. The baryon Hartree propagator is

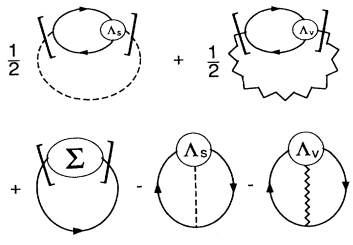

FIG. 1. The two-loop corrections to the RHA energy density. The solid, dashed, and wavy lines represent the baryon Hartree propagator, the free scalar propagator, and the free vector propagator, respectively. The subtractions for the overall divergences and for the vacuum expectation value of the energy are not shown.

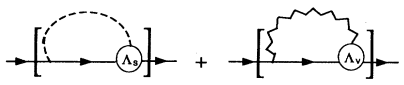

FIG. 2. The proper baryon self-energy. The diagrammatic notation is the same as in Fig. 1.

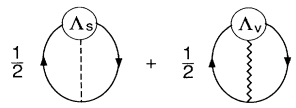

FIG. 3. The unrenormalized two-loop diagrams.

$$G^*(k) = G_F^*(k) + G_D^*(k)\,, \tag{2.4}$$

where

$$G_F^*(k) = \frac{\not{k} + M^*}{k^2 - M^{*2} + i\epsilon}\,, \tag{2.5}$$

$$G_D^*(k) = \frac{i\pi}{E_k^*}(\not{k} + M^*)\delta(k^0 - E_k^*)\theta(k_F - |\mathbf{k}|)\,, \tag{2.6}$$

and the momentum has been shifted to eliminate V_0, which is permissible for the evaluation of closed loops [5]. The free (noninteracting) scalar and vector propagators are

$$\Delta^0(q) = \frac{1}{q^2 - m_s^2 + i\epsilon}\,, \tag{2.7}$$

$$D_{\mu\nu}^0(q) = \left(-g_{\mu\nu} + \frac{q_\mu q_\nu}{m_v^2}\right) D^0(q)\,, \tag{2.8}$$

$$D^0(q) = \frac{1}{q^2 - m_v^2 + i\epsilon}\,. \tag{2.9}$$

By separating the renormalized subdiagrams into unrenormalized parts and counterterm contributions (CTC's), we obtain the more familiar diagrams in Fig. 3, where the CTC's are not shown, since they can be determined easily from Fig. 1. Evidently, an exact evaluation of these loops requires the knowledge of the off-shell proper vertices Λ_s and Λ_v^μ, including their explicit density dependence. These off-shell vertices are currently under investigation [20], but in this work, as a first approximation, we will replace them by their on-shell forms at zero density:

$$ig_s\Lambda_s(q) = ig_s F_s(-q^2)\,, \tag{2.10}$$

$$-ig_v\Lambda_v^\mu(q) = -ig_v\left[F_{v1}(-q^2)\gamma^\mu + iF_{v2}(-q^2)\sigma^{\mu\nu}q_\nu\right]\,, \tag{2.11}$$

where $\sigma^{\mu\nu} = i[\gamma^\mu, \gamma^\nu]/2$, and q^μ is defined as the *incoming* momentum transfer at the vertex. Note that in the calculation of the energy, the on-shell form factors are needed only at *spacelike* momentum transfers, so we can use the results of Ref. [18]. We emphasize that a similar on-shell approximation (with *ad hoc* form factors) is commonly used in essentially all calculations of nuclear matter properties (see, for example, Refs. [15] and [16]); here, however, we will determine the on-shell momentum dependence within the context of our model. This also allows us to discuss some of the implicit density-dependent effects (contained in M^*), which we examine in Sec. V.

With these considerations, we can translate the Feynman diagrams in Figs. 1, 2, and 3 to obtain the renormalized two-loop correction

$$\begin{aligned}\mathcal{E}^{(2)} = {} & \frac{1}{2}g_s^2\int\frac{d^4k}{(2\pi)^4}\frac{d^4q}{(2\pi)^4}\,\mathrm{tr}\,[G^*(k)G^*(k+q)]\,F_s(-q^2)\Delta^0(q) \\ & - \frac{1}{2}g_v^2\int\frac{d^4k}{(2\pi)^4}\frac{d^4q}{(2\pi)^4}\,\mathrm{tr}\,[G^*(k)\gamma_\mu G^*(k+q)\Lambda_v^\mu(q)]\,D^0(q) \\ & + i\int\frac{d^4k}{(2\pi)^4}\,\mathrm{tr}\,[\Sigma_{\mathrm{ct}}G^*(k)] - \sum_{n=1}^{4}\alpha_n\phi_0^n - \mathrm{VEV}\,,\end{aligned} \tag{2.12}$$

where "tr" denotes a trace over spin and isospin indices, and Σ_{ct} contains the counterterms for the baryon self-energy, as given in the Appendix. In Eq. (2.12), we have discarded the longitudinal $q_\mu q_\nu$ term in the vector propagator, since its contribution vanishes by baryon current conservation, as can be easily verified in our approximation. The vacuum-expectation-value (VEV) subtraction is obtained by replacing all of the Hartree propagators $G^*(k)$ with noninteracting Feynman propagators $G_F^0(k) = (\not{k} - M + i\epsilon)^{-1}$ and by omitting the quartic polynomial in ϕ_0. Note that some of the α_n counterterms contain both one-loop $[O(\hbar)]$ and two-loop $[O(\hbar^2)]$ contributions. The one-loop contribution comes from counterterms in the renormalized meson polarizations in Fig. 1. See Eq. (2.79) of Ref. [5] for the details of this separation.

Due to our use of on-shell vertex functions in the two-loop integrals, the renormalization procedure is nonstandard and requires some discussion. In principle, the only unambiguous way to renormalize with vertex insertions is to use the off-shell vertices inside the integrals and include all required counterterms; this is clearly exceedingly difficult and motivates our simplified calculation using the on-shell vertices. We now observe that most of the effort in renormalizing the two-loop integrals with

bare vertices involves the baryon propagators (in the self-energy and polarization loops). The noninteracting meson propagators simply follow along in the analysis, and although they determine which integrals diverge, they are otherwise innocuous. This suggests the following renormalization procedure with dressed vertices.

(1) We first carry out the renormalization of the vertex functions to arrive at finite, on-shell functions of the momentum transfer. This procedure is discussed in the next section, where we specify the detailed form of our model form factors.

(2) To renormalize the baryon self-energy and meson polarizations, we *approximate* the full off-shell vertices by the on-shell forms derived in step 1; these vertices are functions only of the momentum transfer. For the baryon self-energy, this approximation yields the renormalization procedure discussed in Appendix A. For the meson polarizations, the vertex functions *factor out* of the loop integral. The polarizations are then analyzed with the procedure in Ref. [18] by first renormalizing using point vertices and then by multiplying the finite results by the appropriate on-shell vertex functions.

(3) Since the form factors are on shell, we can associate them with the corresponding meson propagators (which carry the same momenta). The form factors then serve only to modify the momentum dependence of the meson propagators, producing so-called "Møller potentials" [28,37].

(4) The counterterms in Eq. (2.12) are then defined exactly as in the two-loop case with bare vertices [5], using the Møller potentials in place of the noninteracting boson propagators.

While this renormalization procedure is not unique, it has the following advantages.

(1) Finite results are obtained with the same number of counterterms as in the original two-loop calculation. All of the counterterms are constants that are defined by vacuum amplitudes, and all counterterm subtractions are *local.*

(2) All subintegrations for the meson polarizations and baryon self-energies satisfy the standard renormalization conditions [5] for any choice of vertex functions.

(3) The resulting energy density satisfies the same renormalization conditions as in the original two-loop calculation, for any choice of vertex functions. In particular, the original results are obtained automatically when the model vertices are replaced by bare vertices. Note that, even with the form factors included, nested and overlapping subtractions remain divergent, although the overall subtractions are finite, as are the baryon self-energy counterterms.

We remark that in a theory that postulates nonlocal vertices in the Lagrangian, the definition of the renormalization counterterms is essentially arbitrary. In particular, since the overall subtractions to the energy are finite, there is no justification for stopping at $O(\phi_0^4)$, and one can simply remove all vacuum fluctuations by fiat. (That is, one can include an infinite number of counterterm subtractions.) To our knowledge, the *only* justification for stopping at a quartic polynomial is that the underlying theory is renormalizable, so that terms of $O(\phi_0^5)$ and higher can never be removed.

Following Ref. [5], we decompose the two-loop contribution into exchange, Lamb-shift, and vacuum fluctuation energies. Thus

$$\mathcal{E}^{(2)} = \mathcal{E}_{\rm EX} + \mathcal{E}_{\rm LS} + \mathcal{E}_{\rm VF} \ , \tag{2.13}$$

where

$$\mathcal{E}_{\rm EX} = \frac{1}{2} g_s^2 \int \frac{d^4k}{(2\pi)^4} \frac{d^4q}{(2\pi)^4} \, {\rm tr}\,[G_D^*(k) G_D^*(k+q)] \, \Delta^0(q) F_s(-q^2) - \frac{1}{2} g_v^2 \int \frac{d^4k}{(2\pi)^4} \frac{d^4q}{(2\pi)^4} \, {\rm tr}\,[G_D^*(k) \gamma_\mu G_D^*(k+q) \Lambda_v^\mu(q)] \, D^0(q) \ , \tag{2.14}$$

$$\mathcal{E}_{\rm LS} = g_s^2 \int \frac{d^\tau k}{(2\pi)^4} \frac{d^\tau q}{(2\pi)^4} \, {\rm tr}\,[G_F^*(k) G_D^*(k+q)] \, \Delta^0(q) F_s(-q^2) + i \int \frac{d^4k}{(2\pi)^4} \, {\rm tr}\,[\Sigma_{\rm ct} G_D^*(k)] - g_v^2 \int \frac{d^\tau k}{(2\pi)^4} \frac{d^\tau q}{(2\pi)^4} \, {\rm tr}\,[G_F^*(k) \gamma_\mu G_D^*(k+q) \Lambda_v^\mu(q)] \, D^0(q) \ , \tag{2.15}$$

$$\mathcal{E}_{\rm VF} = \frac{1}{2} g_s^2 \int \frac{d^\tau k}{(2\pi)^4} \frac{d^\tau q}{(2\pi)^4} \, {\rm tr}\,[G_F^*(k) G_F^*(k+q)] \, \Delta^0(q) F_s(-q^2) + i \int \frac{d^\tau k}{(2\pi)^4} \, {\rm tr}\,[\Sigma_{\rm ct} G_F^*(k)] - \frac{1}{2} g_v^2 \int \frac{d^\tau k}{(2\pi)^4} \frac{d^\tau q}{(2\pi)^4} \, {\rm tr}\,[G_F^*(k) \gamma_\mu G_F^*(k+q) \Lambda_v^\mu(q)] \, D^0(q) - \sum_{n=1}^{4} \alpha_n \phi_0^n - {\rm VEV} \ . \tag{2.16}$$

Here the divergent integrals have been regularized by writing them in τ dimensions, with the limit $\tau \to 4$ taken after the divergences have been removed. Note that, these energy densities are implicitly functions of the baryon density ρ_B and the mass parameter M^*, with the latter to be determined by minimization of the full energy density.

The exchange contribution $\mathcal{E}_{\rm EX}$ is finite. It is straightforward to work out the traces and arrive at the following form that is feasible for numerical integration using Gaussian quadrature:

$$\mathcal{E}_{\rm EX} = \frac{1}{16\pi^4}\int_0^{k_F} dk \int_0^{k_F} dq\, \frac{k^2q^2}{E_k^* E_q^*} \int_{-1}^{+1} dx \left[g_s^2 F_s(P^2) \frac{P^2+4M^{*2}}{P^2+m_s^2} + 2g_v^2 F_{v1}(P^2)\frac{P^2-2M^{*2}}{P^2+m_v^2} + \frac{6g_v^2 M^* F_{v2}(P^2)P^2}{P^2+m_v^2}\right] , \tag{2.17}$$

where we have defined $P^2 \equiv 2(E_k^* E_q^* - M^{*2} - kqx)$, with the dummy variables $k \equiv |\mathbf{k}|$ and $q \equiv |\mathbf{q}|$. (Here and henceforth we take the spin-isospin degeneracy $\gamma = 4$.) Note that, since the momenta flowing through the meson propagators are spacelike, one does not encounter any poles.

The Lamb-shift contribution $\mathcal{E}_{\rm LS}$ can be written as

$$\mathcal{E}_{\rm LS} \equiv -i\int \frac{d^4k}{(2\pi)^4}\,{\rm tr}\,[G_D^*(k)\Sigma_F(k)] \tag{2.18}$$

$$= \left[\Sigma_{FA}(-M^{*2}) + M^*\Sigma_{FB}(-M^{*2})\right]\, 4\int \frac{d^3k}{(2\pi)^3}\frac{M^*}{E_k^*}\,\theta(k_F-|\mathbf{k}|)$$

$$= \left[\Sigma_{FA}(-M^{*2}) + M^*\Sigma_{FB}(-M^{*2})\right]\, \rho_s(M^*;\rho_B) , \tag{2.19}$$

where the renormalized Feynman part of the baryon self-energy is

$$\Sigma_F(k) \equiv \Sigma_{FA}(-k^2) + \not{k}\Sigma_{FB}(-k^2)$$
$$= i\int \frac{d^\tau q}{(2\pi)^4}[g_s^2 G_F^*(k-q)\Delta^0(q)F_s(-q^2) - g_v^2\Lambda_v^\mu(q)G_F^*(k-q)\gamma_\mu D^0(q)] - \Sigma_{\rm ct} , \tag{2.20}$$

and the specification of the counterterm coefficients

$$\Sigma_{\rm ct} \equiv -\zeta_N(\not{k}-M) + \gamma_s\phi_0 + M_c \tag{2.21}$$

is discussed in the Appendix. The scalar density of baryons is denoted by ρ_s.

By following the procedures in Ref. [5], the vacuum fluctuation energy $\mathcal{E}_{\rm VF}$ can be evaluated by expanding the integrands in Eq. (2.16) in powers of (M^*-M) using the algebraic identity

$$G_F^*(k) = \sum_{i=0}^{n}(M^*-M)^i[G_F^0(k)]^{i+1} + (M^*-M)^{n+1}[G_F^0(k)]^{n+1}G_F^*(k) . \tag{2.22}$$

Here n can be any positive integer or zero, and $G_F^0(k)$ is obtained from $G_F^*(k)$ by replacing M^* with M. The zeroth-order term in the expansion $[\mathcal{E}_{\rm VF}(M)]$ is canceled by the VEV, and the counterterms α_n are chosen as usual to cancel exactly the coefficients of the first *four* powers of (M^*-M), which minimizes many-body forces [27,2]. The final result can be written as

$$\mathcal{E}_{\rm VF} = i(M-M^*)^5\int\frac{d^4k}{(2\pi)^4}\,{\rm tr}\left\{[G_F^0(k)]^5G_F^*(k)\Sigma_F^0(k) + [G_F^0(k)]^4G_F^*(k)\Lambda^0(k)\right\}$$
$$+\frac{1}{2}(M-M^*)^5\int\frac{d^4k}{(2\pi)^4}\frac{d^4q}{(2\pi)^4}\,{\rm tr}\big([G_F^0(k-q)]^3G_F^*(k-q)$$
$$\times\{g_v^2\gamma_\mu[G_F^0(k)]^3\Lambda_v^\mu(q)D^0(q) - g_s^2[G_F^0(k)]^3\Delta^0(q)F_s(-q^2)\}\big)$$
$$+\frac{1}{2}(M-M^*)^5\int\frac{d^4k}{(2\pi)^4}\frac{d^4q}{(2\pi)^4}\,{\rm tr}\big([G_F^0(k-q)]^3G_F^*(k-q)$$
$$\times\{g_v^2\gamma_\mu[G_F^0(k)]^2G_F^*(k)\Lambda_v^\mu(q)D^0(q) - g_s^2[G_F^0(k)]^2G_F^*(k)\Delta^0(q)F_s(-q^2)\}\big), \tag{2.23}$$

where $\Sigma_F^0(k)$ is obtained from $\Sigma_F(k)$ by replacing M^* with M, and the renormalized vacuum scalar vertex at zero momentum transfer,

$$\Lambda^0(k) \equiv \Lambda_A^0(-k^2) + \not{k}\Lambda_B^0(-k^2)$$
$$= i\int\frac{d^\tau q}{(2\pi)^4}\{g_s^2[G_F^0(k-q)]^2\Delta^0(q)F_s(-q^2) - g_v^2\Lambda_v^\mu(q)[G_F^0(k-q)]^2\gamma_\mu D^0(q)\} + \frac{\gamma_s}{g_s}, \tag{2.24}$$

is discussed in the Appendix. Note that all integrals in Eq. (2.23) are *finite*, even for point vertices.

After working out the traces, one can perform a Wick rotation to Euclidean momenta and evaluate the angular integrals analytically, leading to ($\widetilde{\mathcal{E}}_{\rm VF} \equiv \mathcal{E}_{\rm VF}/M^4$)

$$\widetilde{\mathcal{E}}_{\rm VF} = \frac{1}{2\pi^2}\int_0^\infty dy\,\frac{(1-m^*)^5 y}{(y+1)^5(y+m^{*2})}\left\{\Sigma^0_{FA}(y)\left[y^3-5(2+m^*)y^2+5(1+2m^*)y-m^*\right]\right.$$
$$\left.+\,\Sigma^0_{FB}(y)\left[(5+m^*)y^2-10(1+m^*)y+1+5m^*\right]y\right\}$$
$$+\frac{1}{2\pi^2}\int_0^\infty dy\,\frac{(1-m^*)^5 y}{(y+1)^4(y+m^{*2})}\left\{\Lambda^0_A(y)\left[(4+m^*)y^2-2(2+3m^*)y+m^*\right]\right.$$
$$\left.-\Lambda^0_B(y)\left[y^2-2(3+2m^*)y+1+4m^*\right]y\right\}$$
$$+\frac{1}{128\pi^4}\int_0^\infty ds\int_0^\infty dt\,\frac{(1-m^*)^5}{(t+1)^3(t+m^{*2})}\left\{\left[t^2-3(m^*+1)t+m^*\right]\left[u_1(s,t)A_1(s)\right.\right.$$
$$\left.\left.-\,v_1(s,t)B(s)\right]+\left[(m^*+3)t\ -3m^*-1\right]\left[u_2(s,t)A_2(s)-v_2(s,t)B(s)\right]\right\}. \tag{2.25}$$

Here we have scaled all dimensional variables with the nucleon mass, set $m^* \equiv M^*/M$, and defined

$$A_1(s) = \frac{g_s^2 F_s(s)}{s+m_s^2} - \frac{4g_v^2 F_{v1}(s)}{s+m_v^2}\ , \tag{2.26}$$

$$A_2(s) = \frac{g_s^2 F_s(s)}{s+m_s^2} + \frac{2g_v^2 F_{v1}(s)}{s+m_v^2}\ , \tag{2.27}$$

$$B(s) = \frac{3g_v^2 F_{v2}(s)}{s+m_v^2}\ , \tag{2.28}$$

and

$$u_1(s,t) = \frac{8st}{Z^3} - \frac{m^* C(s,t)}{(1-m^*)^2} - \frac{5+m^*}{Z}(s+t+1-Z)\ , \tag{2.29}$$

$$u_2(s,t) = \frac{4st}{Z^3}(t-s-1) + \frac{s-t+m^{*2}}{2(1-m^*)^2}C(s,t)$$
$$+\frac{1}{Z}\left[s-t+3-Z+\tfrac{1}{2}(1+m^*)^2\right](s+t+1-Z)\ , \tag{2.30}$$

$$v_1(s,t) = \frac{4st}{Z^3}(t-s+1) - \frac{t-s+m^{*2}}{2(1-m^*)^2}C(s,t)$$
$$-\frac{1}{Z}\left[t-s+3-Z+\tfrac{1}{2}(1+m^*)^2\right](s+t+1-Z)\ , \tag{2.31}$$

$$v_2(s,t) = \frac{4st}{Z^3}(t+s+1) - \frac{m^*(t+s+m^{*2})}{2(1-m^*)^2}C(s,t)$$
$$-\frac{1}{2Z}\left[(5+m^*)(s+t+m^{*2}-Z)+9+2m^*-3m^{*2}\right](s+t+1-Z)\ , \tag{2.32}$$

$$C(s,t) = \sqrt{(s+t+m^{*2})^2-4st} - Z + \frac{1-m^{*2}}{Z}(s+t+1)\ , \tag{2.33}$$

with $Z \equiv \sqrt{(s+t+1)^2-4st}$. We remark that the first two integrals in Eq. (2.25) correspond precisely to the final two integrals in Eq. (2.93) of Ref. [5]. The final integral in Eq. (2.25), however, was obtained here with a new renormalization procedure, and thus it cannot be directly compared to the quadrature in Ref. [5].

The integrals in Eq. (2.25) can be evaluated numerically using Gaussian quadrature. We found that splitting the integrations into two regions in each integral produced results that were accurate to better than 0.1% with a moderate number of points (≈ 32 in each region). The largest uncertainty comes from the final integral in Eq. (2.25). We checked our computations by using two separate computer codes; all results for the nuclear matter energy presented below agreed to at least three digits.

III. SCALAR AND VECTOR VERTEX FUNCTIONS

In the preceding section, we renormalized the two-loop energy with the approximation that the fully off-shell vertices can be replaced by their on-shell forms at zero density, namely, Eqs. (2.10) and (2.11). Here we evaluate these form factors within the framework of our model. Since an exact calculation of the vertex function is impossible at present, we must make approximations. Our strategy is to include in the on-shell vertex functions the dominant physics that is accessible in a hadronic theory.

We begin with the well-known fact that the proper vertex function in QED falls rapidly when the momentum

q^μ entering on the photon line becomes large [29,30]. In particular, the asymptotic form for the on-shell vertex at large spacelike momenta $q^2 < 0$ is

$$\bar{u}(p_b)\Lambda^\mu u(p_a) \longrightarrow \bar{u}(p_b)\gamma^\mu u(p_a) \times \exp\left[-\frac{e^2}{16\pi^2}\ln^2\left(-\frac{q^2}{m^2}\right)\right] , \quad (3.1)$$

where $p_a^2 = p_b^2 = m_e^2$, and m is an infrared regulator mass. In a theory with a *massive* neutral vector boson, the regulator mass m is replaced by the boson mass, and the electron charge e becomes the vector coupling g_v. The physical origin of the strong damping is the large likelihood for virtual bremsstrahlung of soft vector bosons. In diagrammatic terms, the exponential arises from summing all ladders and crossed ladders involving the exchange of soft bosons across the single hard vertex, as shown in Fig. 4. We emphasize that, although the momentum transfer to the vertex is large, the damping arises from the *infrared* structure of the theory, as the required factors of $\ln^2(-q^2)$ are generated by loop momenta that are on the order of the vector meson mass. Thus it is reasonable to include this long-range vertex structure in a renormalizable theory containing hadron loops. Later work supports the assumption that nonleading logarithms appear only as multiplicative factors [31–34].

It is easy to show that the exponential damping in Eq. (3.1) is also reproduced by diagrams in which vector ladders and crossed ladders dress a single (hard) scalar vertex, at least to leading logarithmic order. Since the inclusion of higher-order vertex diagrams involving scalar meson exchanges produces only ultraviolet ("hard") logarithms, as suggested by the work of Appelquist and Primack [35], these diagrams will not ruin the exponential damping [34].

The general forms for the on-shell scalar and vector vertex functions at zero density are given in Eqs. (2.10) and (2.11). Following Ref. [18], we assume that the behavior of both vertices at small $|q^2|$ is determined by the lowest-order vector vertex correction, that is, the middle diagram on the right-hand side of Fig. 4.[1] Then, by knowing the large $|q^2|$ behavior of the form factors, we can interpolate smoothly between the small and large momentum-transfer regimes. Note that we need only spacelike (or Euclidean) momenta to compute the energy, so the form factors should be smooth, which makes the interpolation practical.

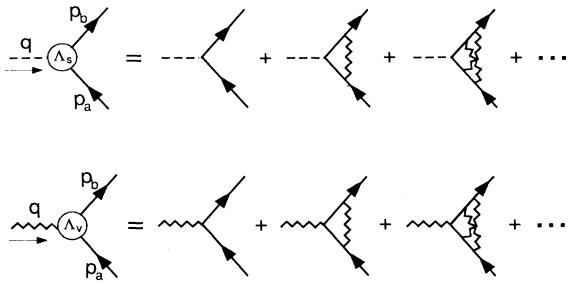

FIG. 4. Diagrammatic expansion of the proper scalar and vector vertices.

The sum of the diagrams for either the scalar or the vector vertex in Fig. 4 results in a rapid suppression at large spacelike momentum transfers. As shown by Fishbane and Sullivan [30], the leading logarithmic asymptotic behavior for the on-shell vector charge form factor at zero density can be written as

$$F_{v1}(-q^2) \longrightarrow \exp\left[F_{v1}^{(1)}(-q^2)\right] , \quad (3.2)$$

where $q = p_b - p_a$ and the superscript "(1)" indicates the lowest-order *correction*. Since the anomalous form factor is suppressed asymptotically by an additional factor of $1/|q^2|$, we can write

$$2MF_{v2}(-q^2) \longrightarrow 2MF_{v2}^{(1)}(0)\frac{1}{|q^2|}\exp\left[F_{v1}^{(1)}(-q^2)\right] , \quad (3.3)$$

where the scale is set by the $O(g_v^2)$ anomalous moment, which is a conservative choice.

At each order in g_v^2, the dressed scalar vertex in Fig. 4 has the same denominator and the same leading power of q^2 in the numerator of the integrand as the dressed vector vertex. Since these features determine the asymptotic behavior [30], we conclude that the scalar and vector vertices behave similarly, and we can therefore write

$$F_s(-q^2) \longrightarrow \exp\left[F_s^{(1)}(-q^2)\right] , \quad (3.4)$$

which again holds for the leading logarithmic behavior.

The lowest-order corrections to the on-shell vector charge and anomalous form factors are evaluated in Ref. [18], and we simply quote the results here:

$$F_{v1}^{(1)}(Q^2) = -\frac{g_v^2}{16\pi^2}\int_0^1 du \left\{\frac{2\left[2(1-u)-u^2+Q^2(1-u/2)^2\right]}{QS(u)}\ln\left[\frac{S(u)+uQ/2}{S(u)-uQ/2}\right] - 2u - \frac{2u\left[2(1-u)-u^2\right]}{u^2+m_v^2(1-u)} + \frac{2S(u)}{Q}\ln\left[\frac{S(u)+uQ/2}{S(u)-uQ/2}\right]\right\} , \quad (3.5)$$

[1] There is also a lowest-order vertex correction involving the exchange of a scalar meson. This additional diagram has a range similar to the diagram that we evaluate, so its inclusion would not significantly change the values that we obtain for the rms baryon radii.

$$2MF_{v2}^{(1)}(Q^2) = \frac{g_v^2}{4\pi^2}\int_0^1 du\,\frac{u(1-u)}{QS(u)}\ln\left[\frac{S(u)+uQ/2}{S(u)-uQ/2}\right], \tag{3.6}$$

where

$$S(u) \equiv \left[u^2 + \frac{u^2Q^2}{4} + m_v^2(1-u)\right]^{1/2}, \tag{3.7}$$

$Q^2 \equiv -q^2/M^2$, $Q \equiv \sqrt{Q^2}$, and m_v is written in units of the baryon mass M.

The lowest-order correction to the on-shell scalar vertex can be calculated analogously. Thus

$$F_s^{(1)}(-q^2) = ig_v^2\int\frac{d^4k}{(2\pi)^4}\gamma^\mu G_F^0(p_b-k)G_F^0(p_a-k)\gamma^\nu D_{\mu\nu}^0(k) + \text{CTC}, \tag{3.8}$$

where the right-hand side is understood to be evaluated on shell ($\not{p}_a = \not{p}_b = M$), and the counterterm contribution (CTC) is determined by imposing the on-shell renormalization condition $F_s^{(1)}(0) = 0$, which insures that the scalar-baryon coupling remains g_s when the momentum transfer is zero. Straightforward manipulations similar to those for the vector vertex [18] yield

$$F_s^{(1)}(Q^2) = -\frac{g_v^2}{16\pi^2}\int_0^1 du\left\{\frac{12S(u)}{Q}\ln\left[\frac{S(u)+uQ/2}{S(u)-uQ/2}\right] - 12u - \frac{4u(1-u+u^2)}{u^2+m_v^2(1-u)} + \frac{2\left[2(1-u+u^2)+Q^2(1-u+\frac{1}{2}u^2)\right]}{QS(u)}\ln\left[\frac{S(u)+uQ/2}{S(u)-uQ/2}\right]\right\}. \tag{3.9}$$

It is not hard to show [18] from Eqs. (3.5) and (3.9) that for large Q^2

$$F_{v1}^{(1)}(Q^2),\ F_s^{(1)}(Q^2) \longrightarrow -\frac{g_v^2}{16\pi^2}\ln^2(Q^2/m_v^2), \tag{3.10}$$

to leading order in logarithms. When combined with Eqs. (3.2) and (3.4), this agrees with Eq. (3.1).

As mentioned previously, we want to join the low- and high-momentum-transfer regimes using a smooth interpolation. Evidently, the smaller the region to be interpolated, the more constrained the interpolation. On the other hand, the larger the high-momentum matching point Q_0, the better the leading logarithmic asymptotic behavior. It is impractical, however, to take Q_0 so large that the nonleading logarithms are negligible compared to the leading logarithms. Thus, for a trade-off, we will approximate the nonleading logarithms by the large Q^2 behavior of $F_{v1}^{(1)}(Q^2)$ and $F_s^{(1)}(Q^2)$. That is, we choose Q_0 large enough so that the values of $F_{v1}^{(1)}(Q^2)$ and $F_s^{(1)}(Q^2)$ can be accurately fitted by the function

$$W(Q^2) = -\frac{g_v^2}{16\pi^2}\left[\ln^2(Q^2/m_v^2) + r_1\ln(Q^2/m_v^2) + r_2\right], \tag{3.11}$$

which means that all polynomials in $1/Q^2$ are negligible. For $Q \geq Q_0$, we take the vertex form factors to be given by Eqs. (3.2), (3.3), and (3.4), with the lowest-order corrections replaced by Eq. (3.11).

To minimize the uncertainty in the interpolations, one wants to choose Q_0 as small as is feasible, and we chose $Q_0 = 5$, as in Ref. [18]. The r_i parameters in Eq. (3.11) were determined by making a least-squares fit to the expressions in (3.5) and (3.9).[2] To test the sensitivity to the nonleading logarithmic behavior, we obtained one set of parameters for $5 \leq Q \leq 40$, and then obtained another ("exact") set by letting $Q^2 \to \infty$. (The exact r_1 and r_2 can be determined analytically in principle, but the numerical evaluation is sufficiently accurate for our purposes.) Our first least-squares fit yields $r_1 \approx -0.235$ and $r_2 \approx -1.60$ for the scalar vertex, and $r_1 \approx -2.88$ and $r_2 \approx 5.76$ for the vector vertex, while the exact results are $r_1 = 0$ and $r_2 = -3.35$ for the scalar vertex, and $r_1 = -3.00$ and $r_2 = 6.66$ for the vector vertex. (These values assume $m_v = 783\,\text{MeV}$ and $M = 939\,\text{MeV}$.) The resulting interpolations for the two choices of r_i (as well as for $r_1 = r_2 = 0$) are nearly indistinguishable, which implies a very small sensitivity to the nonleading logarithmic behavior; for esthetic reasons, we will use the "exact" parameters in all interpolations henceforth.

In Ref. [18], the last two terms in Eq. (3.11) were approximated by introducing a single parameter α such that the asymptotic behavior is $\exp[-(g_v^2/16\pi^2)\ln^2(Q^2/\alpha m_v^2)]$. For the scalar vertex, this is not as conservative as our present method. (That is, the method of Ref. [18] leads to a scalar vertex function that decays *more* rapidly with increasing Q.) We

[2] We note that the onset of the asymptotic regime (Q_0) and the values of the r_i parameters are determined by the behavior of the *integrals* in Eqs. (3.5) and (3.9). Thus these variables are all independent of the strength of the coupling g_v.

therefore use Eqs. (3.2), (3.3), and (3.4) for $Q \geq Q_0 = 5$, with the lowest-order corrections replaced by Eq. (3.11). We take the values of the form factors and their derivatives at $Q = 0$, as given by their lowest-order corrections, together with the values and the derivatives at Q_0, determined from the asymptotic forms, as four input parameters to specify the interpolation functions.

In Ref. [18], the interpolating function was taken as

$$f_M(Q^2) = a\exp(-bQ^2) + c/(1+Q^2) + d\ , \qquad (3.12)$$

where a, b, c, and d are to be determined. This interpolating function contains both Gaussian and monopole terms, so we will call it a "mixed" interpolation for convenience of description. As noticed in Ref. [18], for some values of g_v^2, two different solutions for the parameters a, b, c, and d can be found, while for other values, unique solutions exist. Whereas this behavior can furnish an estimate of the uncertainty in the interpolation, it also results in a nuclear matter energy that is a discontinuous function of g_v^2. This is inconvenient when one attempts to refit the couplings to reproduce nuclear matter saturation.

Thus we use instead the following polynomial interpolating function:

$$f_P(Q^2) = a/(1+Q^2)^3 + b/(1+Q^2)^2 + c/(1+Q^2) + d\ , \qquad (3.13)$$

which yields a unique solution for a, b, c, and d at any g_v^2. To estimate the uncertainties in the interpolation and their effects on the energy density of nuclear matter, we also use the Gaussian interpolating function

$$f_G(Q^2) = a\exp(-Q^2) + b\exp(-Q^2/5) + c\exp(-Q^2/10) + d\ , \qquad (3.14)$$

which also yields a unique solution for a, b, c, and d at any g_v^2. Since $F_{v2}(q^2)$ is suppressed asymptotically by a factor of $1/|q^2|$ relative to $F_{v1}(q^2)$, we take its corresponding interpolating functions to be those of Eqs. (3.13) and (3.14) multiplied by $2MF_{v2}^{(1)}(0)/(1+Q^2)$.

In Fig. 5 we show the scalar form factor and the vector charge form factor using the mixed, polynomial, and Gaussian interpolating functions for RHA couplings. The vector anomalous form factors obtained from Eqs. (3.13) and (3.14) with a further multiplicative factor of $2MF_{v2}^{(1)}(0)/(1+Q^2)$ are shown in Fig. 6(a). The uncertainty envelopes generated by the polynomial and Gaussian interpolations are combined in Fig. 6(b). In Fig. 7(a) we show the vector charge form factor and the corresponding monopole form factor $[F_m(Q^2) = \Lambda^2/(Q^2+\Lambda^2)]$ that decays similarly, while in Fig. 7(b) we show similar results for a dipole form factor $[F_d(Q^2) = \Lambda^4/(Q^2+\Lambda^2)^2]$. The parameters a, b, c, and d for the preceding interpolations are listed in Table I. All values assume $g_v^2 = 102.8$, $m_v = 783\,\mathrm{MeV}$, and $M = 939\,\mathrm{MeV}$.

The preceding figures indicate that the decay of the form factors as a function of Q depends significantly on the interpolation functions. Nevertheless, we have verified that the polynomial and Gaussian forms provide a reasonable envelope on the uncertainty introduced by the interpolation. We will therefore use the polynomial and Gaussian functions to investigate the sensitivity of the nuclear matter binding energy to the decay of the form factors.

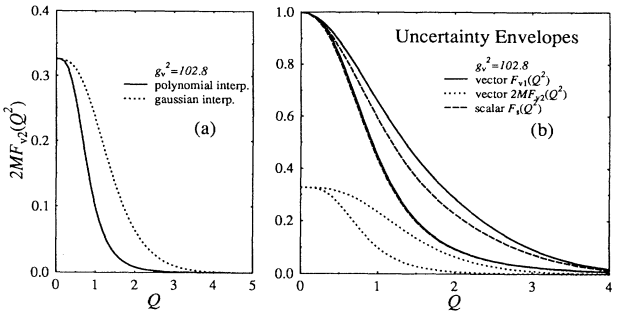

FIG. 6. The on-shell vector anomalous form factor (a) and the uncertainty envelopes generated by the Gaussian and polynomial interpolations (b). The momentum Q is in units of M.

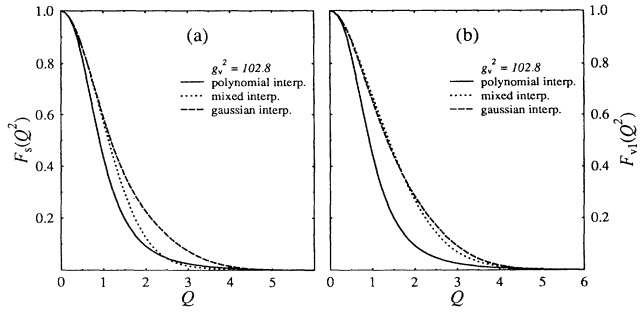

FIG. 5. The on-shell scalar form factor (a) and vector charge form factor (b) with the mixed, polynomial, and Gaussian interpolations. The momentum Q is in units of M.

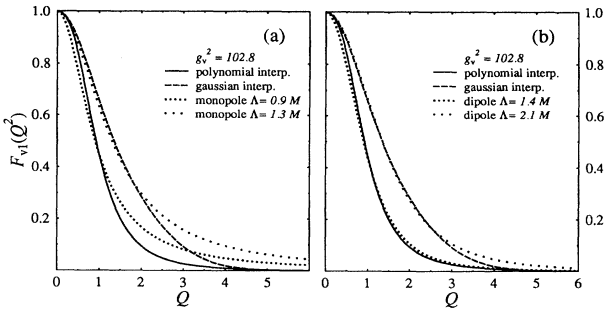

FIG. 7. Comparison of the on-shell vector charge form factor of Fig. 5(b) with some similar monopole and dipole form factors. The momentum Q is in units of M.

TABLE I. Interpolation parameter sets.

		a	b	c	d
Mixed	F_s	0.747185	0.457293	2.60765×10^{-1}	-7.94998×10^{-3}
	F_{v1}	0.792431	0.344247	2.12528×10^{-1}	-4.95969×10^{-3}
Poly.	F_s	−1.30867	2.21488	9.87004×10^{-2}	-4.91063×10^{-3}
	F_{v1}	−1.45088	2.38433	6.92982×10^{-2}	-2.75043×10^{-3}
	F_{v2}	−2.94795	3.98240	-3.35013×10^{-2}	-9.41037×10^{-4}
Gauss.	F_s	0.498343	0.541225	-4.14082×10^{-2}	1.83978×10^{-3}
	F_{v1}	0.348549	0.720836	-7.39583×10^{-2}	4.57337×10^{-3}
	F_{v2}	−1.43842	2.83889	-4.19250×10^{-1}	1.87796×10^{-2}

IV. RESULTS

We now present numerical results for the vertex-corrected two-loop energy computed with the equations in Sec. II and vertices in Sec. III. We start with the results of a perturbative calculation, in which the RHA couplings *and* self-consistent mass M^* are used to compute the two-loop corrections. For convenience of comparison with the results of Ref. [5], we use the couplings $g_s^2 = 54.3$ and $g_v^2 = 102.8$, and masses $m_s = 458\,\mathrm{MeV}$ and $m_v = 783\,\mathrm{MeV}$, which produce nuclear matter equilibrium at $k_F = 1.30\,\mathrm{fm}^{-1}$ with a binding energy/nucleon of 15.75 MeV. Later we present results obtained by refitting the parameters so that the total energy, including the two-loop contributions and the new self-consistent M^*, reproduces the preceding equilibrium properties of nuclear matter. Note that all vertex functions used in this section are fixed at their free-space parametrizations, which follow from the formulas in Sec. III. Calculations both with and without the anomalous form factor F_{v2} will be considered.

The results for the perturbative two-loop energy/baryon of nuclear matter as a function of density, with both the polynomial and Gaussian interpolations for the vertices, are shown in Fig. 8. As a check of our renormalization procedure and numerical calculations, we reproduced the two-loop results with bare vertices as shown in Ref. [5] by setting $F_s = F_{v1} = 1$ and $F_{v2} = 0$.[3] By comparing the results of Fig. 8 with those in Fig. 4 of Ref. [5], we observe that the form factors suppress the vacuum contributions considerably. Moreover, the difference between the two interpolations gives an estimate of the uncertainty in the model vertex functions, which produces large changes on the scale of the nuclear binding energy. Thus the energy density of nuclear matter in this model is sensitive to the behavior of the form factors at intermediate momenta, at least in the two-loop approximation.

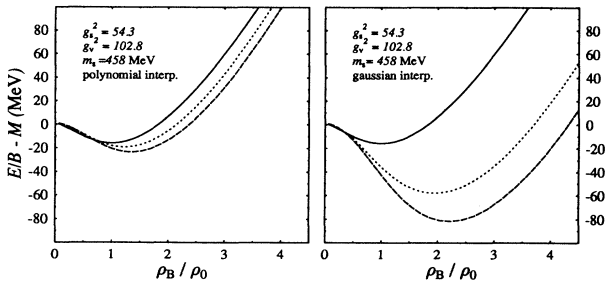

FIG. 8. The perturbative two-loop energy with vertex corrections using the polynomial and Gaussian interpolations. The dotted (dashed) curves are obtained with F_{v2} excluded (included). The solid curve is the RHA energy. Both calculations use RHA parameters and $m_v = 783\,\mathrm{MeV}$. The equilibrium density ρ_0 corresponds to $k_F = 1.30\,\mathrm{fm}^{-1}$.

The separate contributions from the scalar, the vector charge (F_{v1}), and the vector anomalous (F_{v2}) parts are shown in Fig. 9. Evidently, there are strong cancellations between the vector charge and scalar pieces. Notice also that the anomalous contributions are generally only 5%–15% as large as the scalar and vector charge contributions. Nevertheless, the anomalous terms are comparable to the binding energy of nuclear matter and are relevant in a calculation of nuclear matter saturation because of the sensitive cancellations between the vector charge and scalar contributions.

The separate contributions to the two-loop correction from the vacuum fluctuation, the exchange, and the Lamb-shift terms are shown in Fig. 10 with F_{v2} omitted

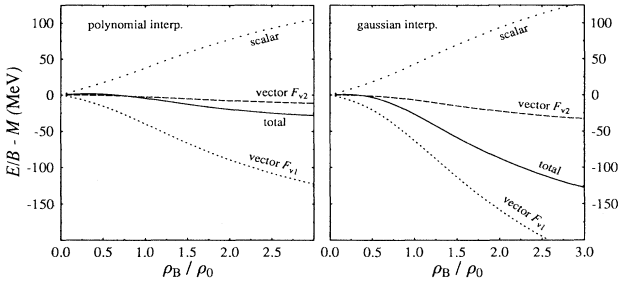

FIG. 9. The separate contributions to the total two-loop correction from the scalar, vector charge, and vector anomalous parts. The parameters are the same as those in Fig. 8.

[3] We can also reproduce the results in Ref. [15] by setting $F_{v2} = 0$ and choosing F_s and F_{v1} equal to the square of the monopole form factors therein.

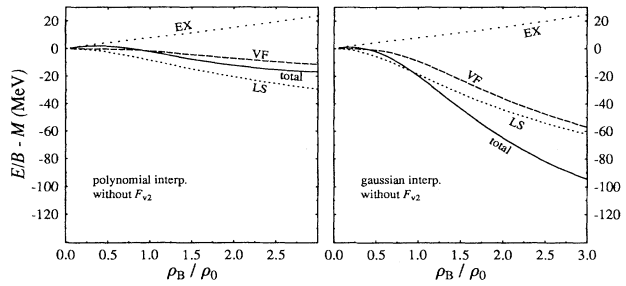

FIG. 10. The separate contributions to the total two-loop correction from the vacuum fluctuation, the exchange, and the Lamb-shift terms, excluding F_{v2}. The parameters are the same as those in Fig. 8.

and in Fig. 11 with F_{v2} included. One observes that the Lamb-shift energy suffers less suppression from the form factors than the vacuum fluctuation energy does. When F_{v2} is included, the vacuum fluctuation and Lamb-shift energies become more negative.

The two-loop energy with vertex modifications $\mathcal{E}^{(1)} + \mathcal{E}^{(2)}$ can be minimized with respect to M^* at each density, and the parameters can be adjusted to reproduce the equilibrium properties of nuclear matter. The vector meson mass is held fixed at its empirical value of 783 MeV (for simplicity), but the scalar meson mass must be increased, with the size of the increase determined by how far the two-loop perturbative result deviates from the RHA result. (If too small a value is chosen for the scalar mass, the resulting interaction is too attractive, and nuclear matter always saturates with too large a binding energy.)

We have found a number of parameter sets that reproduce the equilibrium properties of nuclear matter. A representative sample is listed in Table II, where the compressibility K_v^{-1} is also shown.[4] In general, the compressibility remains large in this approximation and increases

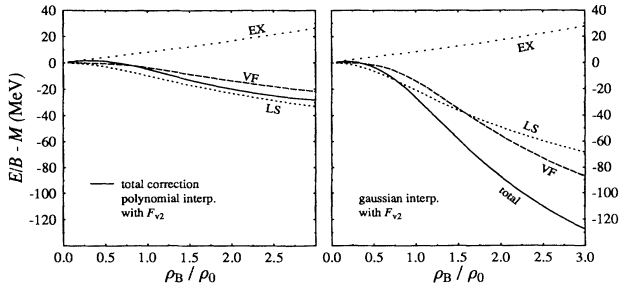

FIG. 11. The separate contributions to the total two-loop correction from the vacuum fluctuation, the exchange, and the Lamb-shift terms, including F_{v2}. The parameters are the same as those in Fig. 8.

[4]As is well known, the compressibility can be reduced, if desired, by including nonlinear scalar meson self-interactions.

TABLE II. Two-loop refitted parameter sets.

Set	Interp.	F_{v2}	g_s^2	g_v^2	m_s (MeV)	K_v^{-1} (MeV)
A	Poly.	No	63.6	130.8	458	600
B	Poly.	Yes	102.6	109.6	600	524
C	Gauss.	No	159.4	79.4	800	437
D	Gauss.	Yes	233.6	106.2	900	494

slightly from the value in the RHA (450 MeV); the form factors with the polynomial interpolation produce more suppression of the vacuum contributions (compared to the Gaussian interpolation), but give a higher compressibility. The corresponding self-consistent nucleon mass is shown as a function of density in Fig. 12. Here M^* is obtained by minimizing the full two-loop energy density $\mathcal{E}^{(1)}(M^*)+\mathcal{E}^{(2)}(M^*)$ with respect to this parameter. The two-loop contributions generally reduce the value of M^*.

To refit the energy/baryon to nuclear matter equilibrium, the scalar mass must be increased significantly, which suggests that the results in this approximation are sensitive to the precise shape of the form factors. Nevertheless, the two-loop calculation with vertex modifications is a better approximation than the conventional two-loop calculation with bare vertices, since the two-loop corrections are smaller, and the refit couplings are of reasonable size. For quantitative comparisons to nuclear matter properties, one must know the form factors more accurately, especially in the intermediate momentum-transfer region. Thus our calculations imply that it is inappropriate to draw conclusions from calculations using some particular *ad hoc* choice of form factors, as in Refs. [15] and [16].

V. RESULTS WITH MEDIUM-MODIFIED VERTICES

One advantage of having an explicit model for the meson-baryon vertex functions is that we can investigate how these functions change in the nuclear medium. For example, the baryon mass changes from M to M^*, and

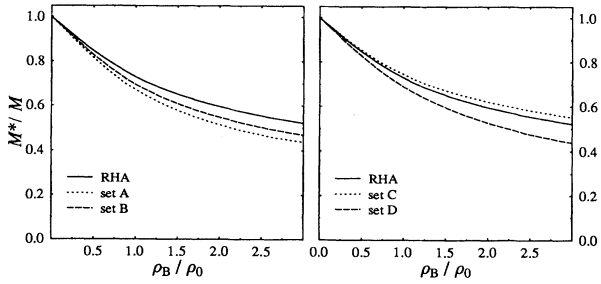

FIG. 12. The effective nucleon mass for the refitted two-loop approximation with vertex modifications obtained for the polynomial and Gaussian interpolations, respectively.

by making this change in the baryon propagators that appear in the vertex loops, the vertex functions acquire an implicit density dependence. This is the effect we will consider in this section. We emphasize that this is a first step in the study of density-dependent vertex modifications in this model, since we are neglecting the valence-nucleon contributions to the vertex loops, as well as additional form factor functions that can arise at finite density. Moreover, as with the calculations in the preceding sections, a quantitative study requires the full off-shell vertex, as well as the inclusion of pions to more accurately describe the long-range vertex structure. We leave these additional modifications as important topics for future investigations. Although the present calculation is just a first step, it illustrates numerous issues that must be dealt with in any microscopic model of the meson-baryon vertices; many of these issues are simply omitted by assumption in conventional calculations based on *ad hoc* form factors.

By replacing M with M^* in the vertex functions, the mass of the virtual intermediate state is reduced, and thus the radius of the dressed nucleon increases with increasing density. This is the primary modification we study here. We emphasize that the leading logarithmic behavior at large spacelike Q^2 is unchanged. However, since we determine the nonleading behavior from an examination of the lowest-order loop diagrams, this behavior also changes at finite density; these effects are very small and are incorporated here just for consistency. We will follow the general strategy described earlier: include effects that can be calculated reliably in our simple model, and treat effects that cannot yet be calculated as conservatively as possible.

It is a straightforward exercise to generalize the results in Sec. II to incorporate the modified baryon mass, and we simply quote the results here:

$$F_s^{*(1)}(Q^2) = -\frac{g_v^2}{16\pi^2}\int_0^1 du \left\{ 12S^*(u)L(u) - 12u - \frac{4u(1-u+u^2)}{u^2+m_v^2(1-u)} + \frac{2\left[2m^{*2}(1-u+u^2)+Q^2(1-u+\frac{1}{2}u^2)\right]}{S^*(u)}L(u) + 8u\ln\left[\frac{m^{*2}u^2+m_v^2(1-u)}{u^2+m_v^2(1-u)}\right]\right\}, \tag{5.1}$$

$$F_{v1}^{*(1)}(Q^2) = -\frac{g_v^2}{16\pi^2}\int_0^1 du \left\{ \frac{2\left\{m^{*2}\left[2(1-u)-u^2\right]+Q^2(1-u/2)^2\right\}}{S^*(u)}L(u) - 2u - \frac{2u\left[2(1-u)-u^2\right]}{u^2+m_v^2(1-u)} + 2S^*(u)L(u) + 2u\ln\left[\frac{m^{*2}u^2+m_v^2(1-u)}{u^2+m_v^2(1-u)}\right]\right\}, \tag{5.2}$$

$$2MF_{v2}^{*(1)}(Q^2) = \frac{g_v^2}{4\pi^2}\int_0^1 du\, \frac{m^*u(1-u)}{S^*(u)}L(u)\,, \tag{5.3}$$

where

$$L(u) \equiv \frac{1}{Q}\ln\left[\frac{S^*(u)+uQ/2}{S^*(u)-uQ/2}\right], \tag{5.4}$$

$$S^*(u) \equiv \left[m^{*2}u^2 + \frac{u^2Q^2}{4} + m_v^2(1-u)\right]^{1/2}, \tag{5.5}$$

$Q^2 \equiv -q^2/M^2$, $Q \equiv \sqrt{Q^2}$, $m^* \equiv M^*/M$, and m_v is written in units of the baryon mass M. We note the important point that the prefactor $2M$ is used solely to make the anomalous contribution dimensionless (any mass could be used), and thus it does *not* change to M^* at finite density.

Here we have renormalized the form factors using the same renormalization conditions as in Sec. III. A straightforward numerical evaluation of the preceding integrals shows that they do not vanish at $Q^2 = 0$, and thus the vector charge and scalar couplings are renormalized at finite density. This is especially surprising for the vector term, since the conservation of the baryon current implies that there is no charge renormalization. The resolution of this dilemma is simple. In a calculation that includes the full off-shell vertex inside the two-loop diagrams, one should also include the appropriate self-energy insertions on the baryon lines to maintain the required Ward identities. Thus, when we "factor out" the vertex from the loop integrations and renormalize it on mass shell, using the procedures discussed in Sec. II, we should *also* extract the self-energies, which now appear on external baryon lines. In free space, these self-energy insertions vanish by construction, due to our choice of

mass and wave-function counterterms, but when M is replaced by M^* one finds a finite wave-function renormalization. It is straightforward to show [36] that the contribution from this wave-function renormalization precisely cancels the shift from $F_{v1}^{*(1)}(0)$, so the baryon number remains unchanged, and baryon number conservation is maintained. Thus we will set the vector charge form factor $F_{v1}^*(0) = 1$ in performing the interpolations discussed below.

The self-energy insertions also produce a finite correction to the baryon mass, which is exactly what is needed to modify the mass in the external spinor to include the correction from the exchange self-energy. Since we will only consider perturbative calculations about the RHA results, in which we neglect all exchange corrections to the baryon mass (by definition), we will neglect this mass shift as well.

In contrast, the scalar vertex is not protected by the Ward identity. The finite wave-function renormalization does not cancel exactly against $F_s^{*(1)}(0)$, and there is a finite shift in the strength of the vertex. However, while we believe that the lowest-order vertex correction gives a reasonable estimate of the form factor radius (since it incorporates the intermediate state with the lowest mass), there is no reason to expect that it is reliable for the renormalization of the scalar coupling strength. This renormalization is a completely dynamical effect that is likely to depend significantly on valence-nucleon contributions, scalar meson exchange diagrams, vacuum polarization, etc., all of which are neglected here. We will therefore take a conservative approach and leave the magnitude of the scalar strength *unrenormalized* at finite density; we postpone the difficult problem of obtaining a reasonable estimate for the finite renormalization to a future investigation.

It is also straightforward to obtain expressions for the medium-modified rms radii of the nucleon, but we will not present the formulas here. (These are most easily obtained by differentiating the Feynman parameter integrals with respect to Q^2, rather than by differentiating the expressions given above.) One finds that the vector charge and scalar mean-square radii scale approximately as $1/M^*$. Because of the overall factor of m^* in $2MF_{v2}^*$, however, the anomalous moment (and its radius) are insensitive to the value of M^*, and this form factor is essentially the same as at zero density.

The parametrizations of the vertex functions are performed as described in Sec. III, with a different parameter set at each value of M^*. One finds that the values of r_1 [see Eq. (3.11)] are unchanged at finite density, while the values of r_2 suffer a (small) change that is exactly the same for the scalar and vector vertex. Figure 13 shows the vector charge form factor at $M^* = 0.7M$, where we have included the finite wave-function renormalization, so that $F_{v1}^*(0) = 1$.

If one faithfully carries out the renormalization procedure defined in Sec. II using the medium-modified vertices, one discovers that the resulting expressions for the two-loop energy are no longer finite. This occurs because the two-loop integrals contain the modified vertices, while the subtraction terms are defined by vacuum

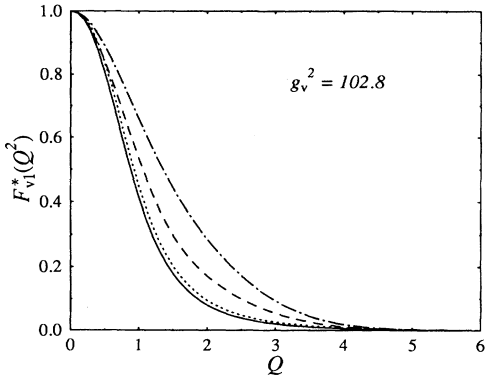

FIG. 13. The vector charge form factor F_{v1}^* at $M^* = 0.7M$. The solid (dashed) line is obtained with polynomial (Gaussian) interpolation. The dotted and dot-dashed lines are the corresponding vacuum form factors with $M^* = M$, which are the same as those in Fig. 5(b). The momentum Q is in units of M.

amplitudes and use unmodified vertices; thus, certain divergences no longer cancel. The problems can be traced to the nested divergences, which require the renormalization of the self-energy and vertex functions, as discussed in the Appendix. (The overlapping subtractions remain unchanged, and the overall subtractions are always chosen to remove the first four powers of ϕ_0.) In principle, the only way to determine the required new subtractions is to use the full off-shell vertices inside the loops. *Within the context of the on-shell approximation for the form factors*, the best that can be done is to use medium-modified vertices for both the two-loop integrals *and* the corresponding subtractions. This is the procedure we follow here; it involves the same strategy as in Sec. II, namely, if it is a reasonable approximation to replace the off-shell vertices with their on-shell forms, it should also be reasonable to use on-shell, medium-modified vertices in performing the subtractions in the present case. The result is that the energy density is calculated by inserting the density-dependent vertex functions, parametrized as discussed earlier, into the expressions for the renormalized two-loop contributions given in Sec. II. (If the on-shell approximation is not a good one, then all of our calculations will have to be improved.)

In Fig. 14, we show the results of a perturbative calculation (RHA parameters and M^*) using the medium-dependent vertices with both the polynomial and Gaussian interpolations. A comparison with Fig. 8 shows that the two-loop corrections are smaller here, as expected from the larger radii (and consequent more rapid decay in momentum space) of the F_{v1}^* and F_s^* vertices. The difference between the results with the two different interpolations is again an estimate of the uncertainty in the form factors at intermediate momenta; these differences remain significant on the scale of the nuclear matter binding energy. Moreover, it is clear that including the density dependence of the vertices also produces effects that are significant on this scale. This suggests that for quantitative calculations of nuclear matter saturation, it

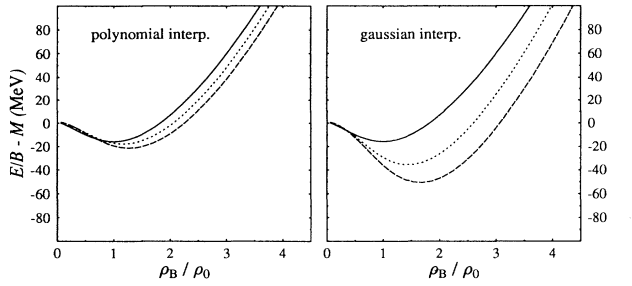

FIG. 14. The perturbative two-loop energy with density-dependent vertices. The couplings are the same as those in Fig. 8. The dotted (dashed) curves are obtained with F_{v2} excluded (included). The solid curve is the RHA energy.

is necessary to include this density dependence, and one can question the accuracy of results using vertices that are simply assumed to be density independent.

VI. SUMMARY

We have calculated the two-loop energy with one dressed vertex for nuclear matter in the Walecka model, using form factors determined in the framework of the model. With an on-shell approximation for the vertex, we determine the leading behavior at large spacelike momentum transfer from the sum of an infinite set of ladder and crossed-ladder diagrams, and we use the lowest-order vertex correction to specify the behavior at small momentum transfer. Two different interpolation functions are used to join the two momentum-transfer regimes. Whereas the resulting vertex functions are not determined uniquely at intermediate momentum transfers and are known only to within an error band, they are specified by the underlying couplings and masses in the model without the introduction of *ad hoc* parameters.

We find that the two-loop corrections to the one-loop energy are considerably smaller than those computed earlier with bare vertices. While these corrections produce significant changes in the nuclear binding energy, one can still fit the empirical equilibrium properties of nuclear matter with a reasonable adjustment of the model parameters. (The most dramatic adjustment is in the scalar meson mass, which must be increased by roughly several hundred MeV.) Since these results were obtained using only one dressed vertex in the loop, it is likely that calculations using two dressed vertices will find even smaller corrections.

We also included the contributions from the anomalous vector vertex for the first time. Although its contribution is small compared to those of the vector charge vertex or the scalar vertex, it is not negligible on the scale of the nuclear matter binding energy. Moreover, the implicit density dependence in the vertices and the uncertainty in our interpolations also produce variations that are important on the scale of the binding energy. These new effects should be present in any realistic model of the meson-baryon vertex functions and must be included before a quantitative calculation of nuclear matter saturation can be performed.

Although the present calculations are the first step in the inclusion of dynamically generated vertex functions in relativistic nuclear matter calculations, and many improvements and refinements must be made, there are several features of our analysis that we believe to be under control. First, the leading logarithmic behavior of the vertices at large spacelike momentum transfer is included correctly. Second, the low-momentum-transfer behavior should be reproduced reasonably well (for a model with only heavy mesons), since we include the intermediate state with the smallest mass. Third, our two different interpolation functions give a realistic "error envelope" for the uncertainty of the vertex functions at intermediate momentum transfer and for the resulting uncertainty in the nuclear matter binding energy. Fourth, the calculated isoscalar anomalous moment has a magnitude that is consistent with empirical values, and thus it provides a meaningful estimate of the size of the isoscalar anomalous contributions to nuclear matter saturation. Finally, the mean-square radii of the vector charge and scalar vertices increase with density roughly as the inverse of the baryon effective mass, which should give sensible results for the impact of this density dependence on the nuclear matter calculation.

There are several improvements that must be made in these calculations before any definitive conclusions can be drawn. First, one must compute the off-shell vertices and include them inside the loop integrals; this will also require a computation of the corresponding self-energies, which must be included to maintain the conservation of the baryon current [20]. Second, the contributions from the density-dependent (valence) parts of the baryon propagators must be included in the computation of the vertex functions; this will introduce (in principle) new vertex functions that arise at finite density. Third, pions must be included to describe the long-range vertex structure more accurately. Fourth, the description of the vertex functions at intermediate momentum transfer should be improved; this may be possible by examining the dispersion relations that determine these functions. Finally, one must investigate the truncation procedure used to define the present approximation to decide if it is more accurate to dress one or both of the vertices in the two-loop terms. All of these improvements can be studied systematically within the QHD framework and provide topics for future work on this problem.

In a larger context, regardless of which degrees of freedom one believes are the most appropriate, it is necessary to have reliable models of the off-shell and density-dependent behavior of the meson-baryon vertices before accurate relativistic calculations of nuclear matter properties can be made. The construction of such models presents a formidable challenge to the practitioners of relativistic nuclear many-body theory.

ACKNOWLEDGMENTS

We are pleased to thank P. J. Ellis, R. J. Furnstahl, C. J. Horowitz, J. Milana, and R. J. Perry for their use-

ful comments. We are also grateful to S. V. Gardner for a careful reading of a draft of this paper. This work was supported in part by the U.S. Department of Energy under Contract No. DE-FG02-87ER40365 and by the National Science Foundation under Grants No. PHY-9203145, No. PHY-9258270, No. PHY-9207889, and No. PHY-9102922.

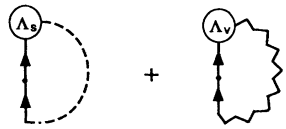

FIG. 15. The baryon-scalar vertex that corresponds to Eq. (2.24).

APPENDIX: BARYON SELF-ENERGY AND BARYON-SCALAR VERTEX

Here we derive the renormalized Feynman parts of the baryon self-energy and baryon-scalar vertex that appear in Eqs. (2.20) and (2.24). The baryon self-energy is shown graphically in Fig. 2. The baryon-scalar vertex is shown in Fig. 15, with the counterterm subtraction omitted. Here we will be interested only in the case of zero momentum transfer. Our renormalization procedure is similar to that in Ref. [7].

It follows from Eq. (2.20) that

$$\Sigma_F(k) = \Sigma_{FA}(-k^2) + \not{k}\Sigma_{FB}(-k^2) \ , \tag{A1}$$

with

$$\Sigma_{FA}(-k^2) = i\int \frac{d^4q}{(2\pi)^4}\,\frac{1}{(k-q)^2 - M^{*2} + i\epsilon}\Big\{g_s^2\Delta^0(q)M^*F_s(-q^2) - g_v^2 D^0(q) \times \left[4M^*F_{v1}(-q^2) + 3(q^2 - k\cdot q)F_{v2}(-q^2)\right]\Big\} - M\zeta_N - \gamma_s\phi_0 - M_c \ , \tag{A2}$$

$$\Sigma_{FB}(-k^2) = \frac{i}{k^2}\int \frac{d^4q}{(2\pi)^4}\,\frac{1}{(k-q)^2 - M^{*2} + i\epsilon}\Big\{\Big[g_s^2\Delta^0(q)F_s(-q^2) + 2g_v^2 D^0(q)F_{v1}(-q^2)\Big](k^2 - k\cdot q) - 3g_v^2 M^* D^0(q)F_{v2}(-q^2)k\cdot q\Big\} + \zeta_N \ . \tag{A3}$$

The convergence properties of these integrals depend on the behavior of the form factors; for bare vertices, the integrals are logarithmically divergent. To renormalize them, we write them in terms of Euclidean momenta and then explicitly subtract the integrands using counterterms chosen to reproduce the appropriate renormalization conditions. (This method is discussed in Refs. [7] and [13].) One can verify that, for bare vertices, this procedure reproduces the results obtained with the more conventional dimensional regularization [5], and it allows us to extend the renormalization to include our model vertex functions.

After making a Wick rotation to Euclidean space ($p_0 \to ip_4^E$) and performing the angular integrals, we can write Eqs. (A2) and (A3) as

$$\Sigma_{FA}(s) = -\frac{1}{64\pi^2 s}\int_0^\infty dt\,\{2[M^*A_1(t) + tB(t)]\Theta_1(s,t;M^{*2}) - B(t)\Phi_1(s,t;M^{*2})\} - M\zeta_N - \gamma_s\phi_0 - M_c \ , \tag{A4}$$

$$\Sigma_{FB}(s) = -\frac{1}{64\pi^2 s^2}\int_0^\infty dt\,\{2sA_2(t)\Theta_1(s,t;M^{*2}) - [A_2(t) + M^*B(t)]\,\Phi_1(s,t;M^{*2})\} + \zeta_N \ , \tag{A5}$$

where $A_1(t), A_2(t)$, and $B(t)$ are defined in Eqs. (2.26), (2.27), and (2.28), and

$$\Theta_1(s,t;m^2) = s + t + m^2 - \left[(s+t+m^2)^2 - 4st\right]^{1/2} \ , \tag{A6}$$

$$\Phi_1(s,t;m^2) = (s+t+m^2)^2 - 2st - (s+t+m^2)\left[(s+t+m^2)^2 - 4st\right]^{1/2} \ . \tag{A7}$$

Here we have set $s = k_E^2$ and $t = q_E^2$, with the subscript "E" denoting Euclidean.

Similarly, from Eq. (2.24), we have

$$\Lambda^0(k) = \Lambda_A^0(-k^2) + \not{k}\Lambda_B^0(-k^2) \ , \tag{A8}$$

with

$$\Lambda_A^0(s) = -\int_0^\infty dt\,\frac{A_1(t)}{32\pi^2 s}\left[\Theta_1(s,t;M^2)+2M^2\Theta_2(s,t;M^2)\right] - \int_0^\infty dt\,\frac{MB(t)}{16\pi^2 s}\left[t\Theta_2(s,t;M^2)-\Phi_2(s,t;M^2)\right]+\frac{\gamma_s}{g_s}\ , \tag{A9}$$

$$\Lambda_B^0(s) = -\int_0^\infty dt\,\frac{MA_2(t)}{16\pi^2 s^2}\left[s\Theta_2(s,t;M^2)-\Phi_2(s,t;M^2)\right] + \int_0^\infty dt\,\frac{B(t)}{64\pi^2 s^2}\left[\Phi_1(s,t;M^2)+4M^2\Phi_2(s,t;M^2)\right]\ , \tag{A10}$$

where

$$\Theta_2(s,t;m^2) = 1-\frac{s+t+m^2}{[(s+t+m^2)^2-4st]^{1/2}}\ , \tag{A11}$$

$$\Phi_2(s,t;m^2) = s+t+m^2-\frac{(s+t+m^2)^2-2st}{[(s+t+m^2)^2-4st]^{1/2}}\ . \tag{A12}$$

The counterterm contributions in Eqs. (A4), (A5), and (A9) are defined by imposing the usual conditions

$$\Sigma_F(p)\big|_{\not p=M=M^*} = 0\ , \tag{A13}$$

$$\frac{\partial}{\partial \not p}\Sigma_F(p)\bigg|_{\not p=M=M^*} = 0\ , \tag{A14}$$

$$\Lambda^0(p)\big|_{\not p=M} = 0\ . \tag{A15}$$

After inserting the expressions for the self-energy and vertex [Eqs. (A1) and (A8)] into Eqs. (A13)–(A15), it is straightforward to find the counterterm contributions and to make the necessary subtractions. After some tedious algebra, the final results are

$$\begin{aligned}\Sigma_{FA}(s) = &-\int_0^\infty dt\,\frac{A_1(t)}{32\pi^2}\left\{\frac{m^*}{s}\Theta_1(s,t;m^{*2})+(2+m^*)t+2m^*-\frac{1}{\eta_t}\left[(2+m^*)t+2(2+3m^*)\right]\right\}\\ &-\int_0^\infty dt\,\frac{A_2(t)}{16\pi^2}\left\{t^2+(2+m^*)t+m^*-\frac{1}{\eta_t}\left[t^2+(4+m^*)t+2+3m^*\right]\right\}\\ &-\int_0^\infty dt\,\frac{B(t)}{64\pi^2}\left\{\frac{2t}{s}\Theta_1(s,t;m^{*2})-\frac{1}{s}\Phi_1(s,t;m^{*2})+t[(6+m^*)t+6m^*]\right.\\ &\left.-\frac{t}{\eta_t}[(6+m^*)t+8(2+m^*)]\right\}\ ,\end{aligned} \tag{A16}$$

$$\begin{aligned}\Sigma_{FB}(s) = &\int_0^\infty dt\,\frac{A_1(t)}{16\pi^2}\left[t+1-\frac{1}{\eta_t}(t+3)\right]\\ &-\int_0^\infty dt\,\frac{A_2(t)}{64\pi^2}\left\{\frac{2}{s}\Theta_1(s,t;m^{*2})-\frac{1}{s^2}\Phi_1(s,t;m^{*2})-(3t^2+8t+4)+\frac{1}{\eta_t}(3t^2+14t+12)\right\}\\ &+\int_0^\infty dt\,\frac{B(t)}{64\pi^2}\left\{\frac{m^*}{s^2}\Phi_1(s,t;m^{*2})+5t^2+6t-\frac{t}{\eta_t}(5t+16)\right\}\ ,\end{aligned} \tag{A17}$$

$$\begin{aligned}\Lambda_A^0(s) = &-\int_0^\infty dt\,\frac{A_1(t)}{32\pi^2}\left\{\frac{1}{s}\Theta_1(s,t;1)+\frac{2}{s}\Theta_2(s,t;1)+t+2-\frac{1}{\eta_t}(t+6)\right\}\\ &-\int_0^\infty dt\,\frac{A_2(t)}{16\pi^2}\left[t+1-\frac{1}{\eta_t}(t+3)\right]\\ &-\int_0^\infty dt\,\frac{B(t)}{16\pi^2 s}\left\{t\Theta_2(s,t;1)-\Phi_2(s,t;1)+\frac{st}{4}\left[t+6-\frac{1}{\eta_t}(t+8)\right]\right\}\ ,\end{aligned} \tag{A18}$$

$$\Lambda_B^0(s) = -\int_0^\infty dt\,\frac{A_2(t)}{16\pi^2 s^2}[s\Theta_2(s,t;1)-\Phi_2(s,t;1)]+\int_0^\infty dt\,\frac{B(t)}{64\pi^2 s^2}[\Phi_1(s,t;1)+4\Phi_2(s,t;1)]\ , \tag{A19}$$

where we have scaled all dimensional variables with the nucleon mass M and defined $\eta_t \equiv \sqrt{1+4/t}$ and $m^* \equiv M^*/M$.

All of the preceding integrals can be evaluated using Gaussian quadrature, although care must be used due to cancellations at large t. It is easily verified that the integrals that contain F_s and F_{v1} are all finite even after setting $F_s = 1$ and $F_{v1} = 1$, while the integrals that contain F_{v2} are also finite when one realizes that, in any realistic calculation, $F_{v2}(s)/F_{v1}(s)$ is suppressed by at least a factor of $1/s$ at large s. We have verified numerically that our results with $F_s = F_{v1} = 1$ and $F_{v2} = 0$ are the same as those of Ref. [5].

[1] J. D. Walecka, Ann. Phys. (N.Y.) **83**, 491 (1974).
[2] B. D. Serot and J. D. Walecka, Adv. Nucl. Phys. **16**, 1 (1986).
[3] B. D. Serot, Rep. Prog. Phys. **55**, 1855 (1992).
[4] R. J. Furnstahl, C. E. Price, and G. E. Walker, Phys. Rev. C **36**, 2590 (1987).
[5] R. J. Furnstahl, R. J. Perry, and B. D. Serot, Phys. Rev. C **40**, 321 (1989).
[6] K. Wehrberger, R. Wittman, and B. D. Serot, Phys. Rev. C **42**, 2680 (1990).
[7] K. Lim, Ph.D. thesis, Indiana University, 1990 (unpublished).
[8] K. Tanaka and W. Bentz, Nucl. Phys. **A540**, 383 (1992).
[9] T. D. Cohen, Phys. Rev. Lett. **62**, 3027 (1989).
[10] R. J. Furnstahl, in *Relativistic Nuclear Many-Body Physics*, edited by B. C. Clark, R. J. Perry, and J. P. Vary (World Scientific, Singapore, 1989), p. 337.
[11] J. F. Dawson and R. J. Furnstahl, Phys. Rev. C **42**, 2009 (1990).
[12] P. J. Redmond, Phys. Rev. **112**, 1404 (1958); P. J. Redmond and J. L. Uretsky, Phys. Rev. Lett. **1**, 147 (1958).
[13] H.-B. Tang, Ph.D. thesis, Indiana University, 1993 (unpublished).
[14] J. Milana, Phys. Rev. C **44**, 527 (1991).
[15] M. Prakash, P. J. Ellis, and J. I. Kapusta, Phys. Rev. C **45**, 2518 (1991).
[16] R. Friedrich, K. Wehrberger, and F. Beck, Phys. Rev. C **46**, 188 (1992).
[17] V. K. Mishra, G. Fai, P. C. Tandy, and M. R. Frank, Phys. Rev. C **46**, 1143 (1992).
[18] M. P. Allendes and B. D. Serot, Phys. Rev. C **45**, 2975 (1992).
[19] G. Krein, M. Nielsen, R. D. Puff, and L. Wilets, Phys. Rev. C **47**, 2485 (1993).
[20] M. P. Allendes, Ph.D. thesis, Indiana University, 1995 (unpublished).
[21] B. A. Freedman and L. D. McLerran, Phys. Rev. D **16**, 1130 (1977); **16**, 1147 (1977).
[22] J. W. Durso, A. D. Jackson, and B. J. Verwest, Nucl. Phys. **A345**, 471 (1980).
[23] W. Lin and B. D. Serot, Phys. Lett. B **233**, 23 (1989).
[24] W. Lin and B. D. Serot, Nucl. Phys. **A512**, 637 (1990).
[25] R. J. Furnstahl and B. D. Serot, Phys. Rev. C **47**, 2338 (1993).
[26] B. D. Serot and H.-B. Tang (unpublished).
[27] S.A. Chin, Ann. Phys. (N.Y.) **108**, 301 (1977).
[28] J. M. Jauch and F. Rohrlich, *The Theory of Photons and Electrons*, 2nd ed. (Springer, New York, 1976), Sec. 12.1.
[29] V. V. Sudakov, Sov. Phys. JETP **3**, 65 (1956).
[30] P. M. Fishbane and J. D. Sullivan, Phys. Rev. D **4**, 458 (1971).
[31] A. Mueller, Phys. Rev. D **20**, 2037 (1979).
[32] J. C. Collins, Phys. Rev. D **22**, 1478 (1980).
[33] A. Sen, Phys. Rev. D **24**, 3281 (1981).
[34] G. Sterman, *Introduction to Quantum Field Theory* (Cambridge University Press, Cambridge, England, 1993), Chap. 12.
[35] T. Appelquist and J. R. Primack, Phys. Rev. D **1**, 1144 (1970).
[36] S. S. Schweber, *An Introduction to Relativistic Quantum Field Theory* (Row, Peterson, and Co., Evanston, IL, 1961), Sec. 15c.
[37] J. D. Walecka, Nucl. Phys. **A399**, 387 (1983).